Solid-State Density Functional Theory Investigation of the Terahertz Spectra of the Structural Isomers 1,2-Dicyanobenzene and 1,3-Dicyanobenzene

Keith C. Oppenheim,[†] Timothy M. Korter,*[,†] Joseph S. Melinger,[‡] and Daniel Grischkowsky[§]

Department of Chemistry, Syracuse University, Syracuse, New York 13244, United States, U.S. Naval Research Laboratory Code 6812, Washington, D.C. 20375, United States, and School of Electrical and Computer Engineering, Oklahoma State University, Stillwater, Oklahoma 74078, United States

Received: August 11, 2010

The high-resolution waveguide terahertz (THz) time-domain spectra (20−100 cm^{-1}) of the two structural isomers 1,2-dicyanobenzene (1,2-DCB) and 1,3-dicyanobenzene (1,3-DCB) have been modeled and assigned using solid-state density functional theory. The THz spectra of these similar molecules are distinctly different in the low-frequency region with the differences being driven by modifications of the crystal packing arrangement between the isomers. Simulations utilizing the hybrid density functionals B3LYP and PBE0 were performed to determine the origins of the observed vibrational features. External lattice vibrations (hindered translations and rotations) are found to dominate these spectra, reinforcing the need for proper solid-state models in the analysis of the THz spectra of organic molecular solids. These calculations were able to account for all of the observed spectral features exhibited by both isomers, even in the case of 1,2-DCB, where the spectrum was found to be the result of two coexisting crystalline polymorphs.

1. Introduction

Terahertz (THz) spectroscopy (10−200 cm^{-1}) has been utilized in a diverse number of scientific applications involving solid-state organic compounds.[1] Terahertz experimental techniques have been applied in the characterization of materials ranging from pharmaceuticals[2] to explosives[3] to create a detailed catalog that can then be used for their detection and identification. These methods have become increasingly popular since THz spectroscopy is a noninvasive and nondestructive means of acquiring the distinctive spectral fingerprints of molecular solids.

The application of THz spectroscopy is dependent upon the confidence that can be achieved in the assignment of observed spectral features to specific molecular motions. Solid-state THz spectra are particularly challenging to model, since the spectra are composed of intramolecular and intermolecular vibrations as well as combinations of these motions. Any successful theoretical method must be able to account for all types of motions simultaneously. Recent publications have shown that solid-state density functional theory (DFT) simulations are an excellent means for the complete assignment of the solid-state THz spectra of crystalline materials.[4,5] The inclusion of crystal-packing interactions in solid-state DFT methods has led to the accurate reproduction of the relevant large-amplitude internal molecular motions in addition to the external crystal-lattice vibrations typically seen in the THz region.[6]

The ability of solid-state DFT to reproduce the THz spectra of similar materials with relatively subtle differences is of great interest. An example of this is in understanding and predicting the THz spectra of crystalline polymorphs where modifications to the solid-state structure may appear minor, but the influence on the physical properties is pronounced.[7] In this study, the structural isomers 1,2-dicyanobenzene (1,2-DCB) and 1,3-dicyanobenzene (1,3-DCB) have been chosen as a benchmark for gauging the performance of solid-state DFT. The THz absorption spectra of these two isomers have previously been reported by Esenturk et al.[8] That important study indicated that all of the observed spectral features below ∼100 cm^{-1} were due to intermolecular vibrations and that solid-state theoretical methodologies were required to fully understand the THz spectra. These molecular solids are particularly important based upon their similarities in both molecular structure and crystal packing arrangement, which provides a stringent test of solid-state DFT methods to properly handle such situations. The packing arrangement of the crystal cell and the solid-state geometries of the 1,2-DCB polymorphs can be seen in Figure 1, while 1,3-DCB is shown in Figure 2. The labeling scheme for both isomers is shown in Figure 3.

The evaluation of these theoretical methods is highly dependent on the quality of the experimental data available. High spectral resolution and narrow line shapes are needed to fully explore the simulation quality. Recent advances in THz spectroscopy have led to the introduction of waveguide terahertz time-domain spectroscopy (waveguide THz-TDS). Waveguide THz-TDS has shown the ability to produce spectra with higher spectral resolution and much narrower line widths than traditional pellet-based THz studies.[9,10] Traditional pressed disk (pellet) THz studies are performed by suspending a small amount of analyte in a matrix of material that does not absorb in the THz region. This method relies on grinding the analyte into a fine crystal powder and attempting to mix it as thoroughly as possible with the matrix. This often leads to irregular crystal fragments and inhomogeneous mixing throughout the pellet. When the THz radiation is passed through the pellet sample, vibrational line broadening and a rising baseline are regularly encountered due to nonresonant light scattering. Unlike pellet THz studies, the waveguide THz-TDS technique dissolves the substance to be studied in a solvent and this is placed between two metal plates with a separation of ∼50 μm. Once the solvent

* To whom correspondence should be addressed. E-mail: tmkorter@syr.edu.
[†] Syracuse University.
[‡] U.S. Naval Research Laboratory Code 6812.
[§] Oklahoma State University.

10.1021/jp107597q
Published on Web 11/04/2010

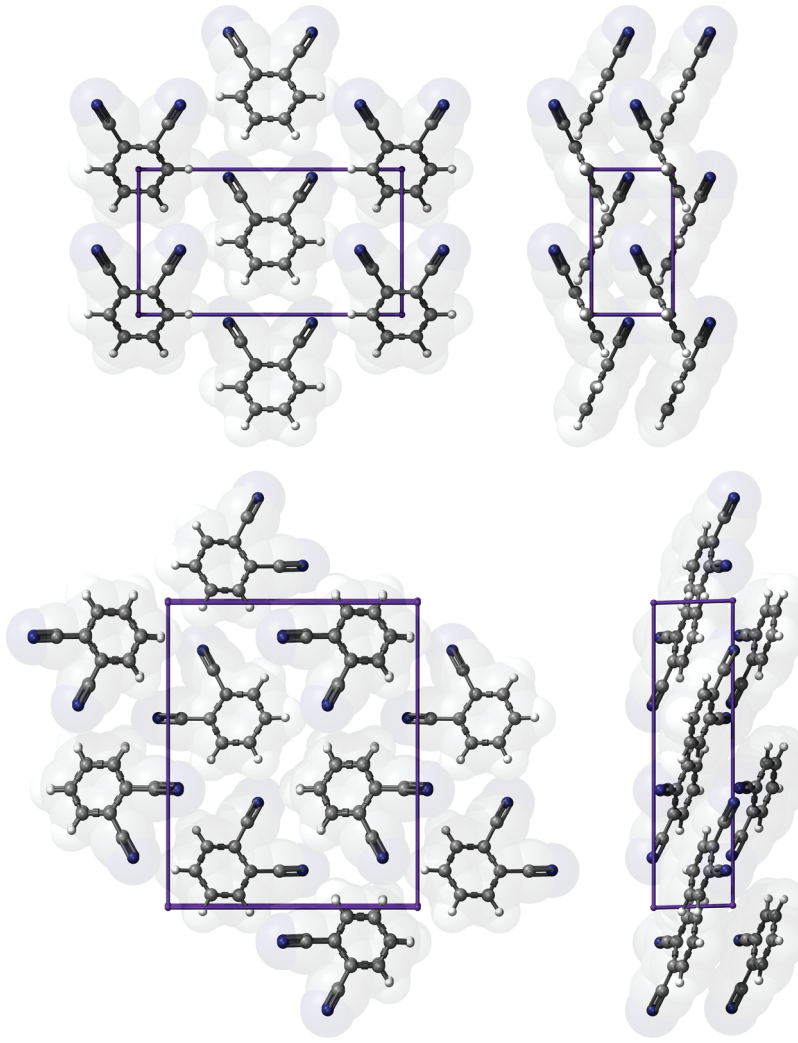

Figure 1. Molecular arrangement and crystal packing of the 1,2-DCB $Z = 2$ polymorph (top panels) and $Z = 4$ polymorph (bottom panels). The left-hand views are along the crystalline *a* axes, and the right-hand images are viewed along the *c* axes.

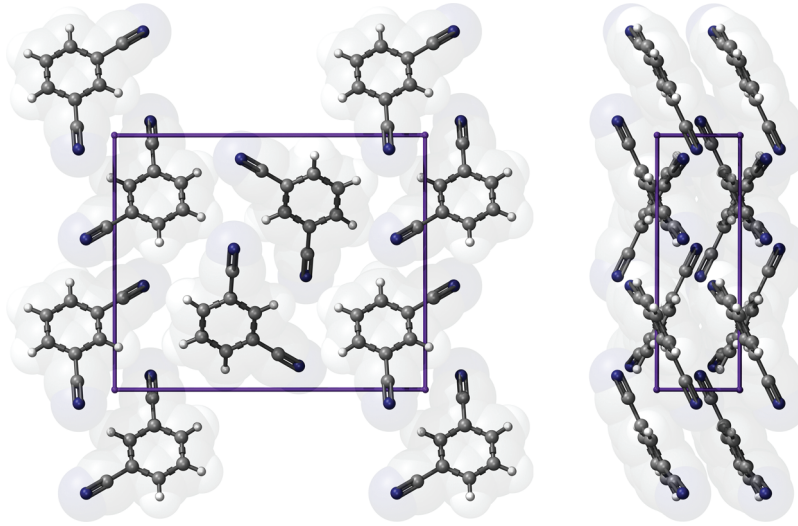

Figure 2. Molecular arrangement and crystal packing of 1,3-DCB. The left-hand panel is a view along the crystalline *a* axis, and the right-hand panel is along the *c* axis.

evaporates, a polycrystalline film is left behind and the THz radiation is propagated between the two metal plates. The increase in spectral resolution that has come from waveguide THz-TDS has led to an opportunity to rigorously test solid-state DFT simulations of organic solids.

2. Experimental and Theoretical Methods

The experimentally determined 12K waveguide THz-TDS spectrum of 1,2-DCB[10] and the 77K spectrum of 1,3-DCB[9] were recorded at Oklahoma State University by drop casting the 1,2-

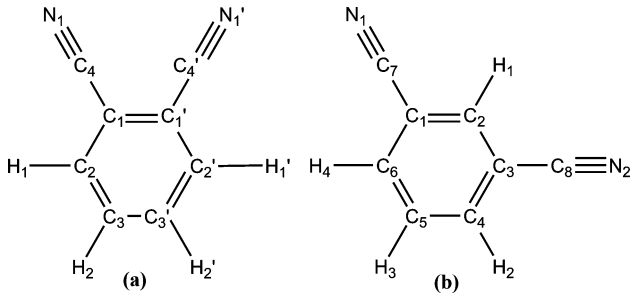

Figure 3. Labeling scheme of the 1,2-DCB (a) and 1,3-DCB (b) molecules.

DCB (in chloroform) and 1,3-DCB (in toluene) onto parallel plate metal waveguides (PPWG): copper in the case of 1,2-DCB and aluminum in the case of 1,3-DCB. Polycrystalline films were formed on the metal plates after evaporation of the solvent. The PPWG was then placed between the THz transmitter and receiver of the spectrometer such that the free-space THz pulses could propagate through the ~50 μm gap and interact with the thin-film crystal material. A description of the THz instrument and additional experimental details are provided elsewhere.[9,10]

The geometry optimizations, harmonic frequencies, and infrared (IR) intensity calculations were performed using the CRYSTAL06[11] program for both solid-state and isolated molecules of 1,3-DCB and 1,2-DCB. All solid-state geometry calculations were performed using the 6-31G(d,p) Gaussian-type basis set.[12] This basis set was paired with two different hybrid density functionals: PBE0[13] and B3LYP.[14,15] These functionals were chosen since they generally outperform generalized gradient approximation density functionals in terms of molecular structure determination.[16] CRYSTAL06 was not used to optimize the lattice parameters; rather, it was used to optimize the molecules within the unit cell under the unit cell constraints and space group symmetry reported by the X-ray diffraction studies found in the Cambridge Structural Database.[17−19] Bond lengths and bond angles were determined from the optimized structures and compared with the experimental crystallography results to gauge the performance of the two density functionals in terms of root-mean-squared-deviation (RMSD) values.

All calculations in this work were performed using the measured crystal lattice parameters reported in previous X-ray studies.[17−19] The 1,2-DCB molecule exhibits two different crystalline polymorphs, both of which are investigated here. The principle distinguishing feature of the two polymorphs is the number of molecules per unit cell. A $Z = 2$ polymorph[17] has been reported at 298 K, and a $Z = 4$ polymorph[19] has been reported at 153 K. The $Z = 2$ polymorph of 1,2-DCB exhibits *Pmn*21 space group symmetry, and the 298 K unit cell parameters are $a = 12.584$ Å, $b = 3.894$ Å, $c = 6.955$ Å, $\alpha = \beta = \gamma = 90°$, and $V = 340.810$ Å^3. The $Z = 4$ polymorph of 1,2-DCB exhibits *P*21/*c* space group symmetry, and the 153 K unit cell parameters are $a = 3.785$ Å, $b = 11.927$ Å, $c = 14.597$ Å, $\alpha = 90°$, $\beta = 91.62°$, $\gamma = 90°$, and $V = 658.704$ Å^3. Only a single polymorph has been reported for crystalline 1,3-DCB.[18] The 1,3-DCB crystal exhibits *P*21/*c* space group symmetry with $Z = 4$, and the unit cell parameters at 298 K are $a = 3.873$ Å, $b = 11.826$ Å, $c = 14.524$ Å, $\alpha = 90°$, $\beta = 94.64°$, $\gamma = 90°$, and $V = 663.049$ Å^3.

Harmonic normal-mode analyses of the two 1,2-DCB polymorphs and 1,3-DCB were then conducted on the final optimized structures. Frequencies were determined by using a mass-weighted numerical evaluation of the Hessian matrix.[20] Infrared intensities were calculated in CRYSTAL06 by determining the Born effective charge tensor using a numerical evaluation of the well-localized Wannier functions of the unit cell.[21] Descriptions of the normal modes were based upon visual inspection of the calculated eigenvectors associated with each vibration.

Several of the software-based convergence parameters were changed to optimize the accuracy and computational time of the calculations. The level of accuracy in the evaluation of the Coulomb and exchange series[20] is composed of five parameters referred to as TOLINTEG in CRYSTAL06.[11] The TOLINTEG threshold values were set to [8 8 8 8 16] for all calculations. The total energy convergence criterion, TOLDEE, was set to 1×10^{-8} hartree for all geometry optimizations and 1×10^{-11} hartree for normal-mode analyses. The atomic grid size used 75 radial points and 974 angular points, which corresponds to the predefined XLGRID size in CRYSTAL06.[11]

Isolated-molecule DFT simulations were also performed using CRYSTAL06 with the B3LYP[14,15] hybrid density functional and the 6-31G(d,p) basis set. The isolated-molecule calculations are used to determine the intramolecular motions of single molecules, and then by comparison with solid-state theory, the crystal packing-induced perturbations may be estimated. The single-molecule calculations are also useful when describing the intramolecular motions found in the solid-state simulations and, when possible, are used as a basis for the unit cell normal-mode descriptions.

3. Results and Discussion

3.1. 1,2-Dicyanobenzene. ***3.1.1. Comparison of the Calculated and Experimental Structures.*** X-ray experimental bond lengths and bond angles are compared to the solid-state calculated results in Table 1 (see Figure 3 for labeling scheme) through the calculated RMSD values. The hydrogen-atom positions determined in an X-ray diffraction study come with a large amount of uncertainty; thus, the C−H covalent bond lengths were not taken into account when determining the RMSD values. All simulations yielded very good agreement with the experimental structures with the maximum RMSD being 0.0118 Å for bonds and 0.2491° for angles. For both 1,2-DCB polymorphs, the PBE0 density functional provided the best reproduction of the bond lengths. It was also found to give better bond angle simulations for the $Z = 4$ polymorph, while the B3LYP simulation was superior for bond angle prediction of the $Z = 2$ polymorph. However, the RMSD values are so similar, making the clear identification of an overall superior density functional not possible.

The existence of two polymorphs for 1,2-DCB may be explained by inspecting the relative energies of the two crystal forms. To make the energies directly comparable between polymorphs, the total calculated electronic energy of each was divided by the Z value of the unit cell. This provides the total energy per unit cell, which represents the relative stability of the two polymorphs. This technique indicates that the $Z = 2$ polymorph is ~3.7 kJ/mol lower in energy than the $Z = 4$ polymorph. This result is surprising since the $Z = 4$ polymorph was expected to be lower in energy given that this is apparently the preferred polymorph at lowered temperatures. The origin of this suspected misordering by the simulations can be found in the experimental unit cell dimensions used in the calculations. The $Z = 2$ polymorph was investigated using a 298 K unit cell size, while the $Z = 4$ simulation is based on a contracted 153 K unit cell. The contracted $Z = 4$ unit cell will drive up the total energy of the solid by imposing increased crystal packing

TABLE 1: Experimental X-ray Diffraction and Theoretical Interatomic Bond Lengths (Å), Bond Angles (deg), and RMSD Values for Two Solid-State 1,2-DCB Polymorphs, $Z = 2$ and 4[a]

	$Z = 2$ polymorph			$Z = 4$ polymorph		
lengths	exp	PBE0	B3LYP	exp	PBE0	B3LYP
C1−C1′	1.401	1.413	1.419	1.408	1.413	1.419
C1−C2	1.378	1.396	1.400	1.387	1.395	1.399
C1−C4	1.430	1.428	1.431	1.444	1.428	1.430
C2−C3	1.354	1.392	1.396	1.385	1.393	1.399
C3−C3′	1.397	1.393	1.396	1.380	1.392	1.396
C4−N1	1.149	1.162	1.164	1.148	1.163	1.164
	RMSD	**0.0102**	**0.0118**		**0.0052**	**0.0104**
angles	exp	PBE0	B3LYP	exp	PBE0	B3LYP
C1−C2−C3	120.31	119.71	119.80	119.59	119.59	119.94
C1−C4−N1	179.52	179.56	179.51	178.86	178.58	179.06
C2−C1−C4	120.74	120.05	120.05	120.92	120.50	119.68
C2−C1−C1′	119.50	119.86	119.78	119.78	119.83	119.71
C2−C3−C3′	120.29	120.43	120.41	120.45	120.58	120.56
C4−C1−C1′	119.78	120.09	120.16	119.21	119.60	120.37
	RMSD	**0.2149**	**0.2048**		**0.1154**	**0.2491**

[a] See Figure 3 for atomic labels. Experimental parameters are from refs 17 ($Z = 2$) and 19 ($Z = 4$).

TABLE 2: Frequency Positions (cm^{-1}) and RMSD Values (cm^{-1}) of the 1,2-DCB ($Z = 4$) Simulations Compared to the Waveguide THz Experiment[a]

THz experiment	PBE0	B3LYP
26.48	21.45 (1.03)	23.12 (1.52)
47.57	34.49 (5.29)	40.68 (6.21)
49.18	44.06 (2.21)	46.87 (3.94)
	54.03 (1.11)	54.61 (1.20)
55.84	57.96 (17.77)	58.82 (17.65)
69.84	64.53 (40.67)	66.63 (35.37)
71.02	64.72 (10.41)	67.85 (9.46)
81.75	75.83 (13.26)	79.06 (14.59)
92.91	83.44 (48.67)	88.62 (49.70)
RMSD	**6.83**	**4.45**

[a] Infrared intensities (km/mol) are shown in parentheses.

TABLE 3: Frequency Positions (cm^{-1}) and RMSD Values (cm^{-1}) of the 1,2-DCB ($Z = 2$) Simulations Compared to the Waveguide THz Experiment[a]

THz experiment	PBE0	B3LYP
26.48	27.95 (0.86)	27.88 (0.90)
47.57	31.22 (0.65)	35.65 (0.64)
49.18		
55.84	39.86 (0.54)	40.86 (0.47)
69.84		
71.02	65.64 (17.73)	68.69 (17.41)
81.75	73.63 (3.45)	75.20 (2.99)
92.91	81.04 (24.91)	84.49 (26.48)
RMSD	**11.26**	**9.02**

[a] Infrared intensities (km/mol) are shown in parentheses.

forces as compared to the 298 K unit cell of the $Z = 2$ polymorph. When the unit cells have such similar energies (~3.7 kJ/mol), it is very likely that even small changes in the unit cell dimensions can lead to a reordering of the relative energies. Thus, the relative stabilities of the two 1,2-DCB polymorphs cannot be unambiguously established, but they are certainly energetically similar.

3.1.2. Comparison of the Theoretical and Experimental Vibrational Frequencies. The solid-state geometry-optimized structures were used as the basis for the normal-mode analysis and THz spectral simulation of the two 1,2-DCB polymorphs. The frequency positions for both polymorphs are compared to the experimental waveguide THz-TDS results and listed in Tables 2 and 3. Since the $Z = 2$ polymorph occurs at room temperature and the waveguide THz-TDS spectrum was recorded at 12 K, it was likely that the sample was primarily composed of the $Z = 4$ polymorph. The $Z = 4$ polymorph simulations predict nine IR-active modes in the low-frequency region, while there are eight visible features in the experimental THz spectrum (though the asymmetries in the features near 70 and 95 cm^{-1} suggest they consist of a superposition of underlying lines). The frequency RMSD values were calculated by assigning eight of the calculated modes (based on IR intensity) to absorption maxima in the experiment. The B3LYP density functional clearly outperformed the PBE0 simulation by resulting in an RMSD value that was ~33% lower. The B3LYP simulation provided good overall results when compared to the experiment as shown in Table 2, but upon closer study of the spectra, it became obvious that there was an issue with missing spectral intensity particularly near 95 cm^{-1}. To address this missing absorption, the $Z = 2$ polymorph THz simulation was investigated.

The simulations for the $Z = 2$ polymorph are compared to the experimentally determined results in Table 3. The $Z = 2$ polymorph only predicts six normal modes in the low-frequency region studied. This is a definite indication that the $Z = 2$ polymorph alone cannot explain the features observed. This is also evident from the high RMSD values which suggest that the correlations made between theory and experiment are inadequate. However, the real value in the $Z = 2$ simulation is not in its ability to account for all of the spectral intensity in the THz spectrum of 1,2-DCB, but rather in its ability to explain the anomalous intensity near 95 cm^{-1} in the experimental spectrum.

In Figure 4, the experimental results are compared with the B3LYP theoretical spectral predictions for both 1,2-DCB polymorphs and also a 2:1 ($Z = 4$:$Z = 2$) linear combination of the two polymorphs. The PBE0 results are represented in the same fashion in Figure 5. The theoretical predictions are shown in stick form with an empirical Lorentzian line shape (1.5 cm^{-1} full-width half-maximum) to improve the visual representation of the data. These figures show that the THz spectrum of 1,2-DCB is likely the superposition of the THz spectra of two separate 1,2-DCB polymorphs. While the $Z = 4$ simulation offers a good reproduction of most spectral features, visual inspection of the data displayed in Figures 4 and 5 suggest

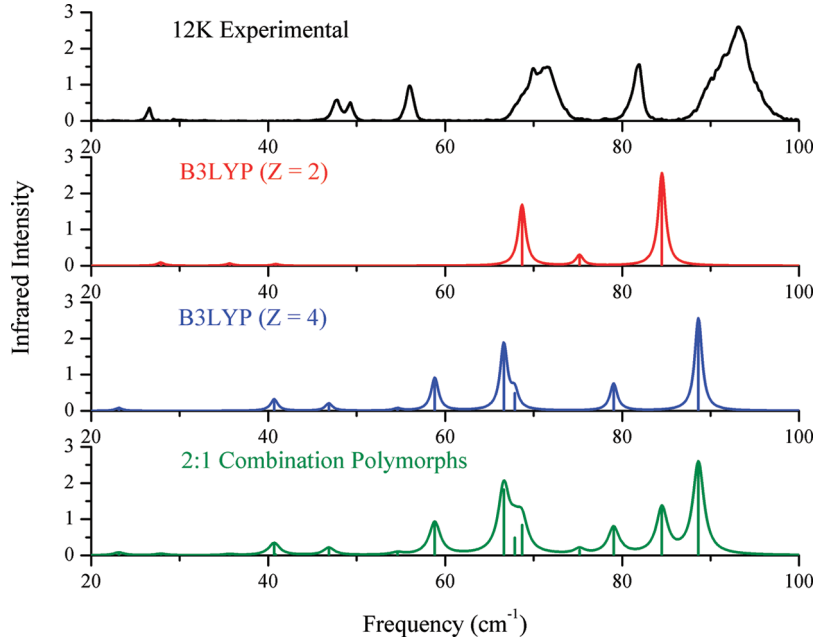

Figure 4. Comparison of the experimental and simulated solid-state 1,2-DCB THz spectra using the B3LYP simulations. The combination trace is a 2:1 ratio of a linear combination of the $Z = 4$ and 2 simulations. Calculated IR intensities have been normalized to the experimental scale. An empirical 1.5 cm^{-1} full-width half-maximum Lorentzian line shape has been convolved with the theoretical data to aid visual comparison.

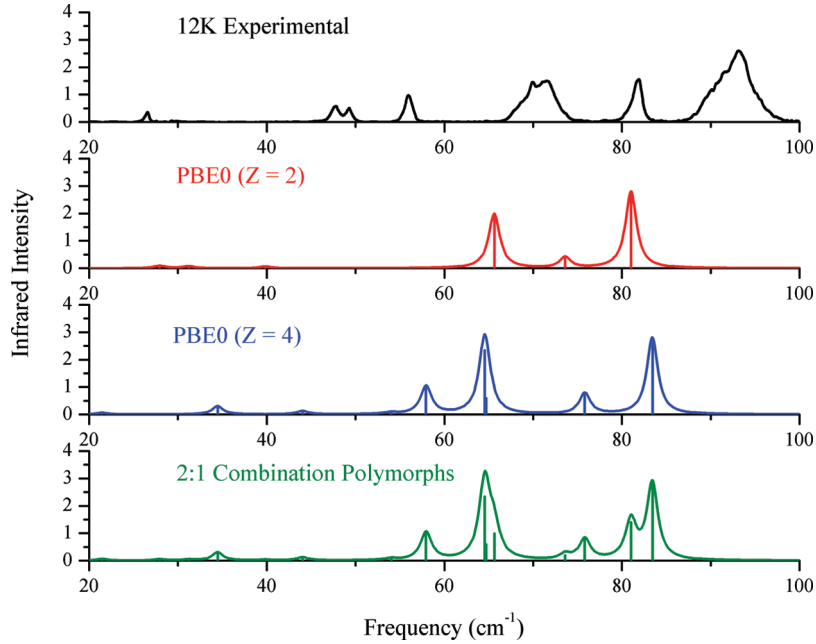

Figure 5. Comparison of the experimental and simulated solid-state 1,2-DCB THz spectra using the PBE0 simulations. The combination trace is a 2:1 ratio of a linear combination of the $Z = 4$ and 2 simulations. Calculated IR intensities have been normalized to the experimental scale. An empirical 1.5 cm^{-1} full-width half-maximum Lorentzian line shape has been convolved with the theoretical data to aid visual comparison.

the $Z = 2$ polymorph is needed to explain the unusual line width near 95 cm^{-1}. A 2:1 (~66% $Z = 4$, ~33% $Z = 2$) combination of the two polymorphs yields a reasonable overall simulated spectrum for 1,2-DCB using either density functional. The coexistence of both 1,2-DCB polymorphs is consistent with their relative energies being similar as discussed earlier.

3.1.3. Temperature Dependence of the 1,2-DCB THz Simulations. The temperature dependence of the 1,2-DCB simulated spectrum is an important factor to consider in the accurate assignment of the observed spectral features. Each polymorph was simulated using higher temperature ($Z = 2$ at 298 K and $Z = 4$ at 153 K) unit cell dimensions than what the experimental spectra were measured at (12 K). If the unit cells of the 1,2-DCB polymorphs were compressed to mimic the effects of cooling, the features should increase in energy to yield an even better theoretical representation of the experimental data. In order to have more confidence in these unit cell volume manipulations, several simulations were performed by changing the volume of the $Z = 2$ polymorph. The $Z = 2$ polymorph was chosen for this volume test since the only available crystallographic data was reported at 298 K, and therefore, it should display the greatest sensitivity to this simple temperature-dependence model. The cell volume of the X-ray diffraction study was decreased evenly by −1.5% (335.698 $Å^3$) and −2.0% (333.994 $Å^3$). A crystal cell undergoing a temperature change would not likely change dimensions in a linear fashion, but these

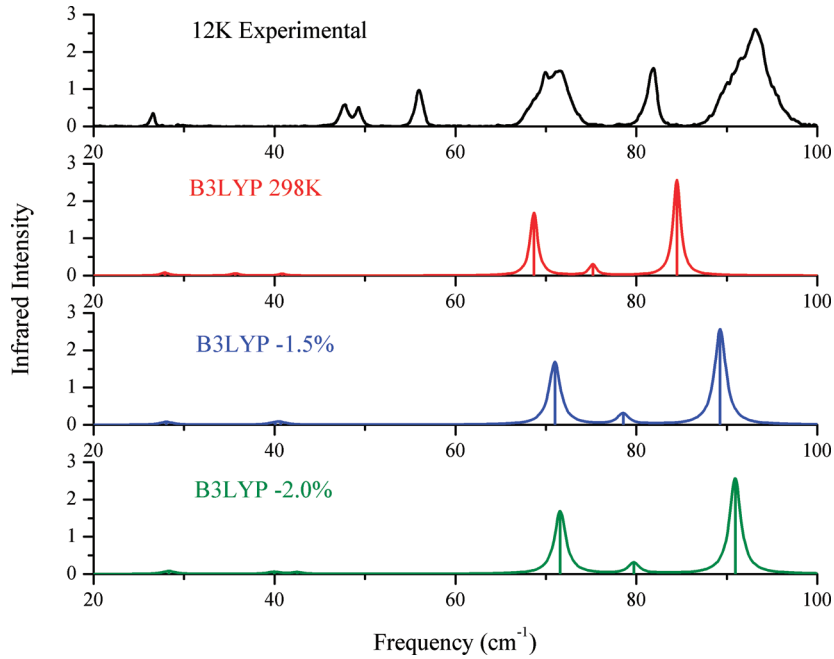

Figure 6. Comparison of the experimental 1,2-DCB ($Z = 2$) THz spectra with the B3LYP room-temperature simulation and the −1.5% and −2.0% reduced crystal cell simulations. An empirical 1.5 cm^{-1} full-width half-maximum Lorentzian line shape has been convolved with the theoretical data to aid visual comparison.

parameters were used to approximate how the frequencies may change in this type of environment. The experimental spectrum is shown against the B3LYP room-temperature simulation and the −1.5% and −2.0% unit cell simulations in Figure 6. This data clearly shows a shift to higher energy by the normal modes when the cell is constricted, as is expected by the lowering of temperature.

Many of the predicted vibrations align much better with the experimental data with the cell contraction applied. The ν_6 mode is a good example of this, where it moves from ∼84 to ∼89 cm^{-1} in the −1.5% volume change cell. This shift would put this mode directly in line with the shoulder seen in the highest energy feature of the experimental spectrum. This is even more pronounced in the −2.0% volume change simulations. The RMSD frequency values change significantly for the $Z = 2$ polymorph when the cell size is changed. The RMSD changes from the room temperature cell value of 8.41 to 7.02 cm^{-1} when the cell undergoes a −1.5% volume change. The simulation yields an RMSD of 6.44 cm^{-1} when the cell is constricted further to −2.0%. The significant improvement in the frequency RMSD values by simulating the effects of lowered temperature reveal that unit cells used as the basis for these calculations should be measured at temperatures as similar to the spectroscopic temperatures as possible. While expansion and contraction of the unit cells by arbitrary scaling factors may better reproduce the THz spectra, they are not a complete replacement for the proper experimental determination of the unit cell parameters.

3.1.4. Mode Descriptions. From the simulations presented here, it has been shown that a very good reproduction of the experimental data can be attained by combining both polymorphs in the overall description of the observed 1,2-DCB spectrum. Since the normal modes have been assigned to features seen in the experimental results, the nature of the origins of the spectral features can now be explored.

While it is well established that the isolated-molecule simulations are generally inappropriate for the reproduction of solid-state THz spectra, they are still commonly found in the literature to assign THz spectra. While not useful for absolute spectral assignments, they can be used to determine how great a perturbation is experienced by internal modes when included in a periodic solid. However, in the case of 1,2-DCB, the isolated-molecule simulations indicated that no IR-active modes are present in the THz region. The two lowest IR-active internal vibrations of the isolated molecule were calculated to be at 113.64 and 115.34 cm^{-1}. None of these isolated-molecule vibrations were seen in the solid-state simulations below 100 cm^{-1} and therefore are not relevant to the mode descriptions provided here.

The IR-active vibrations that form the THz spectrum of 1,2-DCB are all intermolecular external modes. The mode descriptions for both the $Z = 2$ and the $Z = 4$ polymorph, between 20 and 100 cm^{-1}, were performed by visual inspection of the eigenvector displacements. Table 4 lists the low-frequency mode descriptions for the $Z = 2$ polymorph, while Table 5 details the mode descriptions for the $Z = 4$ polymorph. It is important to note that the modification of unit cell volumes for the $Z = 2$ polymorph did not result in any distinguishable changes in the normal-mode eigenvectors.

3.2. 1,3-Dicyanobenzene. ***3.2.1. Comparison of the Calculated and Experimental Structures.*** The solid-state calculated and X-ray experimental bond lengths and bond angles and corresponding RMSD values for the 1,3-DCB molecule are presented in Table 6 (see Figure 3 for labeling scheme). The PBE0 and B3LYP hybrid density functionals both produced structures in very good agreement with the X-ray diffraction-determined experimental structure. The PBE0 simulation yielded the lowest bond distance RMSD overall, 0.0102 Å, but bond angles were best reproduced by the B3LYP calculation. The structural RMSD values indicate that hybrid density functionals provide very good overall accuracy of bond length and bond angle parameters and therefore offer a realistic simulation of the solid-state structure. Due to the excellent performances of both hybrid functionals, both were used as theoretical bases for the simulation and assignment of the experimental THz spectrum of 1,3-DCB.

TABLE 4: Calculated IR-Active Solid-State Modes for 1,2-DCB ($Z = 2$) Low-Frequency Normal Modes[a]

mode	mode description	room-temperature frequency (cm^{-1})
ν_1	external: optical translation along the *a* axis	27.879
ν_2	external: optical translation along the *b* axis	35.652
ν_3	external: rotation of molecules about the *a* axis (out of phase for $Z = 2$ unit cell)	40.856
ν_4	external: rotation of molecules about the *b* axis (in phase for $Z = 2$ unit cell)	68.686
ν_5	external: rotation of molecules about the *a* axis (out of phase for $Z = 2$ unit cell)	75.199
ν_6	external: rotation of molecules about the *a* axis (in phase for $Z = 2$ unit cell)	84.491

[a] All frequencies were determined using the B3LYP functional.

TABLE 5: Calculated IR-Active Solid-State Modes for 1,2-DCB ($Z = 4$) Low-Frequency Normal Modes[a]

mode	mode description	frequency (cm^{-1})
ν_1	external: rotation of molecules about the *c* axis (in phase for $Z = 4$ unit cell)	23.124
ν_2	external: rotation of molecules about the *c* axis (out of phase for $Z = 4$ unit cell)	40.677
ν_3	external: rotation of molecules about the *b* axis (out of phase for $Z = 4$ unit cell)	46.874
ν_4	external: rotation of molecules about the *b* axis (in phase for $Z = 4$ unit cell)	54.608
ν_5	external: rotation of molecules about the *c* axis (out of phase for $Z = 4$ unit cell)	58.817
ν_6	external: rotation of molecules about the *a* axis (out of phase for $Z = 4$ unit cell)	66.627
ν_7	external: rotation of molecules about the *a* axis (in phase for $Z = 4$ unit cell)	67.849
ν_8	external: rotation of molecules about the *c* axis (in phase for $Z = 2$ unit cell)	79.064
ν_9	external: rotation of molecules about the *c* axis (out of phase for $Z = 4$ unit cell)	88.617

[a] All frequencies were determined using the B3LYP functional.

3.2.2. Comparison of the Theoretical and Experimental Vibrational Frequencies. The B3LYP and PBE0 hybrid density functionals provided very good agreement with the observed bond distances and bond angles, but the frequency positions for each theoretical THz spectrum must be examined to determine which simulation predicts the normal modes of 1,3-DCB the most accurately. The solid-state normal-mode-simulated frequencies are compared to the experimental results in Table 7. The simulated IR intensities (km/mol) are shown in parentheses for each density functional for numerical comparison.

Table 7 shows that the waveguide THz-TDS spectrum contains four spectral features below 100 cm^{-1}. Each simulation predicts four highly intense IR-active modes in this same region. The RMSD values are large for the 1,3-DCB simulation despite the confidence of having the correct theory−experiment correlations based on intensity and splitting patterns. The intensity distributions found in the simulations reasonably match the experimental intensity pattern, and the splitting of the first three IR-active modes further supports their assignments. The large frequency RMSD values are primarily caused by the significant underestimation of ν_4 by both density functionals.

TABLE 6: Experimental X-ray Diffraction and Theoretical Interatomic Bond Lengths (Å), Bond Angles (deg), and RMSD for Solid-State 1,3-DCB[a]

bond length	experiment	PBE0	B3LYP
C1−C2	1.372	1.397	1.401
C2−C3	1.379	1.397	1.401
C3−C4	1.393	1.402	1.406
C4−C5	1.373	1.390	1.393
C5−C6	1.368	1.389	1.392
C6−C1	1.384	1.402	1.410
C1−C7	1.434	1.430	1.430
C3−C8	1.430	1.430	1.433
C7−N1	1.148	1.162	1.163
C8−N2	1.139	1.162	1.164
	RMSD	**0.0102**	**0.0122**
bond angles	**experiment**	**PBE0**	**B3LYP**
C1−C2−C3	119.2	118.4	118.6
C2−C3−C4	120.6	120.9	120.9
C3−C4−C5	119.2	119.6	119.6
C4−C5−C6	120.5	120.4	120.5
C5−C6−C1	120.1	119.5	119.6
C6−C1−C2	120.5	121.0	120.9
C6−C1−C7	120.1	119.3	119.4
C2−C1−C7	119.4	119.7	119.7
C2−C3−C8	120.0	119.4	119.4
C4−C3−C8	119.4	119.7	119.7
C1−C7−N1	178.6	178.8	178.8
C3−C8−N2	179.6	179.5	179.5
	RMSD	**0.3365**	**0.2950**

[a] See Figure 3 for atomic labels. Experimental values are from ref 18.

TABLE 7: Frequency Positions (cm^{-1}) and RMSD Values (cm^{-1}) of the 1,3-DCB Simulations Compared to the Waveguide THz Experiment[a]

	THz experiment	PBE0	B3LYP
ν_1	44.40	33.21 (5.18)	36.12 (3.50)
ν_2	55.12	48.40 (9.77)	51.21 (5.95)
ν_3	70.00	58.80 (23.43)	65.50 (30.73)
ν_4	90.67	69.83 (16.43)	74.28 (14.70)
	RMSD	**13.54**	**9.71**

[a] Infrared intensities (km/mol) are shown in parentheses.

Figure 7 shows the four IR-active features seen in the experimental spectrum along with the B3LYP and PBE0 theoretical simulations displayed in stick form along with an empirical Lorentzian line shape (1.5 cm^{-1} full-width half-maximum) to improve the visual representation. As is clear from Figure 7 and Table 7, the PBE0 simulation is shifted to much lower frequency as compared to both the experimental data and the B3LYP results. While the general intensity distribution calculated by the PBE0 density functional is reasonable, the great underestimation of the normal-mode frequencies makes for a very poor representation of the experimental THz spectrum of 1,3-DCB. This provides a good example of a particular density functional that is able to generate an excellent solid-state structure, but fails at producing a proper THz spectral simulation. The best performing density functional in the case of both dicyanobenzenes investigated here is B3LYP, since it is able to simultaneously predict high-quality solid-state structures and low-frequency vibrations.

3.2.3. Temperature Dependence of the 1,3-DCB THz Simulations. In order to help verify the peak assignments, the 1,3-DCB crystal cell was decreased by −1.5% from the room-temperature volume in order to simulate the effects of the temperature difference between experiment (77 K) and theory

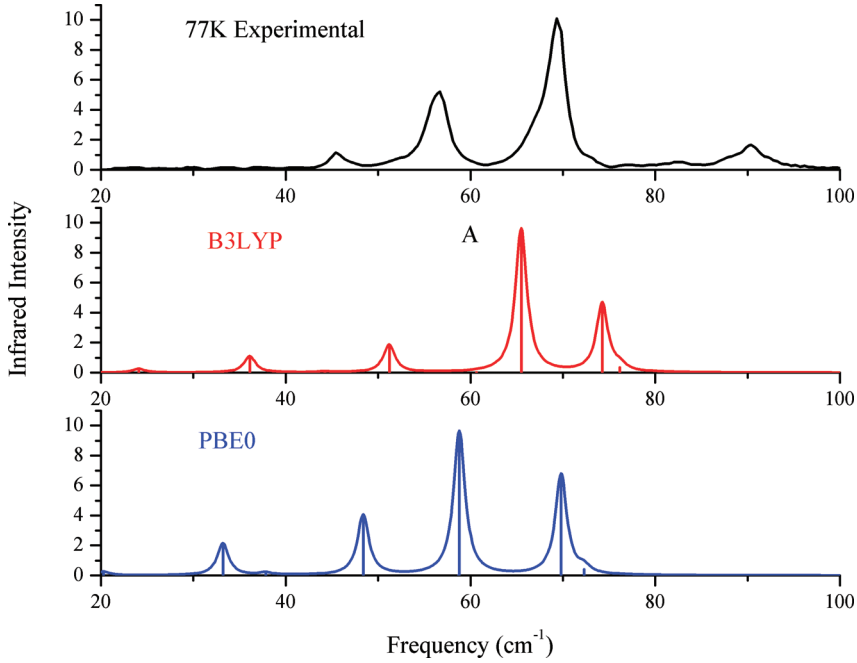

Figure 7. Comparison of the experimental 1,3-DCB THz spectrum with the B3LYP and PBE0 simulations. An empirical 1.5 cm^{-1} full-width half-maximum Lorentzian line shape has been convolved with the theoretical data to aid visual comparison.

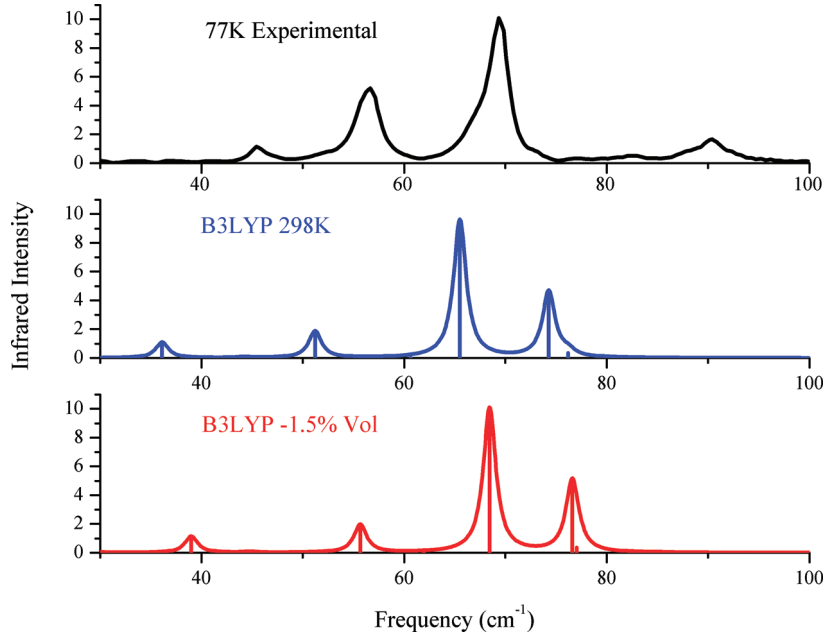

Figure 8. Comparison of the experimental 1,3-DCB THz spectra with the B3LYP 298 K simulation and the −1.5% reduced unit cell volume simulation. An empirical 1.5 cm^{-1} full-width half-maximum Lorentzian line shape has been convolved with the theoretical data to aid visual comparison.

(298 K). The B3LYP functional, which had the lowest structural RMSD value and showed the best agreement of its simulated spectra to the data in Figure 7, was chosen to simulate the volume change.

The change in volume greatly reduced the frequency RMSD value for 1,3-DCB from 9.7 to 7.6 cm^{-1}. The results of the cell volume change simulations are shown in Figure 8. The significant repositioning of all the calculated vibrations to higher energy upon unit cell contraction suggests that much of the observed error in the simulations is due to temperature-related problems. The proper unit cell dimensions based on a real determination of a 77 K 1,3-DCB unit cell would likely result in further reduced frequency RMSD values.

3.2.4. Mode Descriptions of 1,3-DCB. While the positions of each simulated frequency do not align exactly with the experimental spectrum, the IR intensity trends along with the frequency shifts from the contracted unit cell volume calculations make it so that assignments to the four observed features may be made confidently. The normal-mode character of the THz vibrations of crystalline 1,3-DCB were all identified as external intermolecular rotations and translations with the lowest frequency isolated-molecule mode calculated at 117.36 cm^{-1}. The internal modes are well outside the spectral range of interest discussed here and therefore are discussed no further. The descriptions of the four assigned normal modes are listed in Table 8 as calculated using B3LYP.

TABLE 8: Solid-State Frequencies and Mode Descriptions of the Four Normal-Mode Vibrations Seen in the THz Region of 1,3-DCB

mode	frequency (cm^{-1})	intensity (km/mol)	mode description
ν_1	36.1	3.50	external: in-phase molecular rotation about the *a* axis, plus translation along the *y* axis
ν_2	51.2	5.95	external: out-of-phase rotation about the *b* axis
ν_3	65.5	30.73	external: in-phase rotation about the *a* axis
ν_4	74.3	14.70	external: out-of-phase rotation about the *b* axis

4. Conclusions

The cryogenic high-resolution waveguide THz-TDS spectra of the two structural isomers 1,2-DCB and 1,3-DCB have been assigned using solid-state DFT calculations. The B3LYP and PBE0 hybrid different density functionals with the 6-31G(d,p) basis set were utilized, and excellent structural agreement with the room-temperature X-ray experimental results was found for each. Normal-mode analyses of the solid-state structures enabled a full assignment of all the observed spectral features to be accomplished. For 1,3-DCB, the simulation of the THz spectrum was very good using the B3LYP density functional and clear assignments could readily be made. The simulation of the 1,2-DCB THz spectrum was more challenging, since the observed spectral features could not be explained by a single polymorph. It was found that the THz spectrum was composed of absorptions due to coexisting $Z = 4$ and 2 crystalline polymorphs, each with a unique set of THz vibrations. The $Z = 4$ polymorph was found to be dominant with a population ratio of approximately 2:1 over the $Z = 2$ polymorph.

While B3LYP simulations enabled the complete assignment of the THz spectra of both dicyanobenzene isomers to be accomplished, most of the theoretical frequencies were shifted to lower frequency than those observed in the experimental THz results. Additional DFT calculations were performed on 1,2-DCB and 1,3-DCB using contracted unit cell parameters which resulted in a shift of the simulated features to higher frequency, which yielded better frequency RMSD values. This demonstrates the sensitivity of THz vibrational frequencies to temperature through modification of unit cell dimensions and that the selection of unit cell parameters must be done carefully.

Acknowledgment. The authors gratefully acknowledge support from Syracuse University, the National Science Foundation CAREER Program (CHE-084705), and the Defense Threat Reduction Agency (09-2438M).

References and Notes

(1) Beard, M. C.; Turner, G. M.; Schmuttenmaer, C. A. *J. Phys. Chem. B* **2002**, *106*, 7146.
(2) Taday, P. F. *Philos. Trans. R. Soc. London, Ser. A: Math., Phys. Eng. Sci.* **2004**, *362*, 351.
(3) Kemp, M. C.; Taday, P. F.; Cole, B. E.; Cluff, J. A.; Fitzgerald, A. J.; Tribe, W. R. *Proc. SPIE: Int. Soc. Opt. Eng.* **2003**, 44.
(4) Allis, D. G.; Fedor, A. M.; Korter, T. M.; Bjarnason, J. E.; Brown, E. R. *Chem. Phys. Lett.* **2007**, *440*, 203.
(5) Allis, D. G.; Prokhorova, D. A.; Korter, T. M. *J. Phys. Chem. A* **2006**, *110*, 1951.
(6) Allis, D. G.; Korter, T. M. *Int. J. High Speed Electron. Syst.* **2007**, *17*, 193.
(7) *Polymorphism in Pharmaceutical Solids*, 2nd ed.; Informa Healthcare: New York, 2009.
(8) Esenturk, O.; Evans, A.; Heilweil, E. J. *Chem. Phys. Lett.* **2007**, *442*, 71.
(9) Melinger, J. S.; Laman, N.; Harsha, S. S.; Cheng, S.; Grischkowsky, D. *J. Phys. Chem. A* **2007**, *111*, 10977.
(10) Melinger, J. S.; Laman, N.; Harsha, S. S.; Grischkowsky, D. *Appl. Phys. Lett.* **2006**, *89*, 251110/1.
(11) Dovesi, R.; Saunders, V. R.; Roetti, C.; Orlando, R.; Zicovich-Wilson, C. M.; Pascales, F.; Civalleri, B.; Doll, K.; Harrison, N. M.; Bush, I. J.; D'Arco, Ph.; Llunell, M. *CRYSTAL06 User's Manual*; University of Torino: Torino, 2006.
(12) Hehre, W. J.; Ditchfield, R.; Pople, J. A. *J. Chem. Phys.* **1972**, *56*, 2257.
(13) Adamo, C.; Barone, V. *J. Chem. Phys.* **1999**, *110*, 6158.
(14) Becke, A. D. *J. Chem. Phys.* **1993**, *98*, 5648.
(15) Stephens, P. J.; Devlin, F. J.; Chabalowski, C. F.; Frisch, M. J. *J. Phys. Chem.* **1994**, *98*, 11623.
(16) Allis, D. G.; Korter, T. M. *ChemPhysChem* **2006**, *7*, 2398.
(17) Janczak, J.; Kubiak, R. *Acta Crystallogr., Sect. C: Cryst. Struct. Commun.* **1995**, *C51*, 1399.
(18) Janczak, J.; Kubiak, R. *J. Mol. Struct.* **2000**, *553*, 157.
(19) Lynch, V. Personal Communication.
(20) Pascale, F.; Zicovich-Wilson, C. M.; Gejo, F. L.; Civalleri, B.; Orlando, R.; Dovesi, R. *J. Comput. Chem.* **2004**, *25*, 888.
(21) Zicovich-Wilson, C. M.; Pascale, F.; Roetti, C.; Saunders, V. R.; Orlando, R.; Dovesi, R. *J. Comput. Chem.* **2004**, *25*, 1873.

JP107597Q